Dehghany, J., Hoboth, P., Ivanova, A., Mziaut, H., Müller, A., Kalaidzidis, Y., Solimena, M., Meyer-Hermann, M.

A Spatial Model of Insulin-Granule Dynamics in Pancreatic β-Cells

(2015) Traffic, 16 (8), pp. 797-813.

A spatial model of insulin-granule dynamics in pancreatic β-cells

Jaber Dehghany,[1,a] Peter Hoboth,[2,3] Anna Ivanova,[2,3] Hassan Mziaut,[2,3] Andreas Müller,[2,3] Yannis Kalaidzidis,[4,5] Michele Solimena,[2,3,4] Michael Meyer-Hermann[1,6,b]

[1)] *Department of Systems Immunology and Braunschweig Integrated Centre of Systems Biology, Helmholtz Centre for Infection Research, 38124 Braunschweig*

[2)] *Paul Langerhans Institute Dresden of Helmholtz Centre Munich at University Clinic Carl Gustav Carus of TU Dresden and Faculty of Medicine, Technische Universität Dresden, Dresden, Germany*

[3)] *German Center for Diabetes Research (DZD e.V.), Neuherberg, Germany*

[4)] *Max Planck Institute of Molecular Cell Biology and Genetics, Dresden, Germany*

[5)] *Faculty of Bioengineering and Bioinformatics, Moscow State University, Moscow, Russia*

[6)] *Institute for Biochemistry, Biotechnology and Bioinformatics, Technische Universität Braunschweig, Braunschweig, Germany*

Abstract

Insulin secretion from pancreatic β-cells in response to sudden glucose stimulation, is biphasic. Prolonged secretion *in vivo* requires synthesis, delivery to the plasma membrane (PM) and exocytosis of insulin secretory granules (SGs). Here, we provide the first agent-based space-resolved model for SG dynamics in pancreatic β-cells. Using recent experimental data, we consider a single β-cell with identical SGs moving on a phenomenologically represented cytoskeleton network. A single exocytotic machinery mediates SG exocytosis on the PM. This novel model reproduces the measured spatial organization of SGs and insulin secretion patterns under different stimulation protocols. It proposes that the insulin potentiation effect and the rising second-phase secretion are mainly due to the increasing number of docking sites on the PM. Furthermore, it shows that for 6 min after glucose stimulation, the “newcomer” SGs are recruited from a region within less than 600 nm from the PM.

Keywords: agent-based model, β-cell, biphasic insulin secretion, diabetes, granule dynamics, newcomer, potentiation

I. Introduction

Insulin is secreted from pancreatic β-cells in response to raised levels of plasma glucose. The secretory response to increased glucose exhibits two temporally resolved phases: a transient peak lasting for only a few minutes, followed by a much lower but sustained secretion that lasts as long as glucose stimulation continues. This *biphasic insulin secretion* (1) has attracted attention in experimental and theoretical studies (2–7). The selective loss of the first secretion phase is a prominent hallmark of Type 2 diabetes (8–11). Moreover, the second secretion phase is reduced in diabetic β-cells (1, 8, 12). Therefore, understanding the mechanisms behind biphasic insulin secretion and how the structural and dynamical properties of the β-cells contribute to or change during secretion is of great importance and can guide the development of suitable drugs for diabetes treatment.

Different experiments (13–17) have shown that the first phase of insulin secretion mainly relies on the exocytosis of insulin secretory granules (SGs) that are already docked to the plasma membrane (PM) before stimulation (called "pre-docked" SGs). Using total internal reflection fluorescence microscopy (TIRFM), it has been shown that during 4 min of glucose

[a] jadeh@theoretical-biology.de
[b] mmh@theoretical-biology.de

stimulation of murine β-cells, ≈75% of the fusion events were caused by pre-docked SGs (17). Selective removal of pre-docked SGs in the same cells led to 50% reduced secretion in the first phase (17). A few minutes after glucose stimulation, when the number of pre-docked SGs became considerably less (15), insulin secretion continued at a lower rate. During this second phase, secretion was due to exocytosis of "newcomer" SGs, which docked to the PM after stimulation began (1, 15, 17). The term "newcomer" refers to the SGs which have been absent or dimly visible and appear *de novo* after stimulation within the evanescent field of TIRFM and then undergo exocytosis (4, 18). The term "readily releasable pool" (RRP) of granules (1) refers to a dynamic group of SGs which are release-competent. The RRP is replenished continuously by secretion and SG dynamics. Thus, before stimulation, the terms "RRP" and "pre-docked" apparently refer to the same SG group (5), whereas during stimulation, the RRP loses some pre-docked SGs and recruits some "newcomers". The two phases of secretion can be separated using non-nutrient stimuli like K^+, which in the absence of glucose, predominantly evoke the first phase of secretion (13) with a decreasing tail instead of a sustained second phase (19). However, the average depth (distance from the PM) from which the newcomer SGs are recruited for exocytosis during the second phase is still unclear. This will be addressed with the mathematical model presented here.

Since the first observation of biphasic insulin secretion in the 1960s (20), several elaborate mathematical models (21–30) have been proposed for stimulation–secretion coupling in β-cells. The generally accepted model is called the pool-limited (or storage-limited) model in which the population of SGs is made up of different pools (1, 5, 19, 25). These pools dynamically exchange SGs at rates which can differ between the resting and stimulated states (26–28). These models have successfully reproduced the characteristics of biphasic secretion and compare well with experimental findings. For example, they confirm that the first and the second phases of secretion are mainly due to pre-docked and newcomer SGs, respectively, (27, 28, 31, 32). However, none of these models has provided a spatial representation of SG organisation and motility in the β-cell. Recent advances in TIRFM have provided a growing body of knowledge about spatio-temporal dynamics in β-cells, from SGs (4, 17) to exocytotic machinery (33–35). Spatial models of β-cells are needed to gain a predictive capacity based on these measurements. A spatial model not only relates the rate parameters of inter-pool SG exchange to their measured dynamics, but also better estimates the variations of these rates under different stimulations or drug treatments. For example, studying the effect of selective destruction of cytoskeleton network elements on the number of exocytosis events (insulin secretion) clearly needs a three-dimensional spatial model. This is because the extent of the variations of "rates" in an alternative model of differential equations, after destruction of the cytoskeleton network, would be unknown. The same holds true for the average depth from which the newcomer SGs are recruited to the PM. In short, morphology–secretion relations can be only analysed and compared with ultrastructural measurements in space-resolved models.

With modern experimental methods, it is difficult to monitor SG dynamics in the whole β-cell. Imaging of exocytosis events by TIRFM is restricted to 40–100 nm (17, 25), the penetration depth of the evanescent waves of TIRFM (36). These experimental limitations are a major obstacle in understanding the contribution of SGs in different states and positions to insulin secretion. We propose that a space-resolved and mechanistic *in silico* description of SG dynamics can improve our understanding of insulin secretion, provided it is based on firm experimental data. The agent-based model presented here (see below), to our

knowledge, is the first spatial β-cell model of SG homeostasis and dynamics. It is built on experimental data of β-cell morphology and homeostatic SG distribution (37), SG dynamics (38) and stimulated insulin secretion (1). The model covers SG dynamics including biosynthesis, SG motility on the cytoskeleton network (microtubules and actin filaments, which are phenomenologically represented), SG docking and fusion. Moreover, the small number of SGs which undergo exocytosis per minute during both phases of insulin secretion (1, 39, 40), together with the recent finding that only 5000–6000 SGs exist per β-cell (37, 41), emphasises the importance of stochastic effects, which are a natural part of the agent-based model but have not been addressed in the space-averaged differential equation methods (27, 28, 31, 32) due to their deterministic nature. Our space-resolved stochastic agent-based model is validated with quantitative data of insulin secretion and used further to shed light on the aforementioned unresolved questions.

II. Model and assumptions

We developed a spatial β-cell model in which SGs (agents) move on and interact with the cytoskeleton. Even though SGs follow the same decision-making rules, each SG behaves differently, depending on position, size and time, thus generating heterogeneous SGs in different states. Such heterogeneity can make the collective behaviour of SGs complex, despite their common behavioural rules. A diagram of the β-cell features considered in the model is provided in Figure 1. In the following subsections, the main assumptions of the model are explained.

A. β-cell morphology

A spherical β-cell with a R = 6 µm radius (surface area 452.4 µm^2) and a spherical nucleus with a R_n = 3.1 µm radius is assumed (39). The cell cortex, where actin filaments (AFs) facilitate SG motility, is defined as a

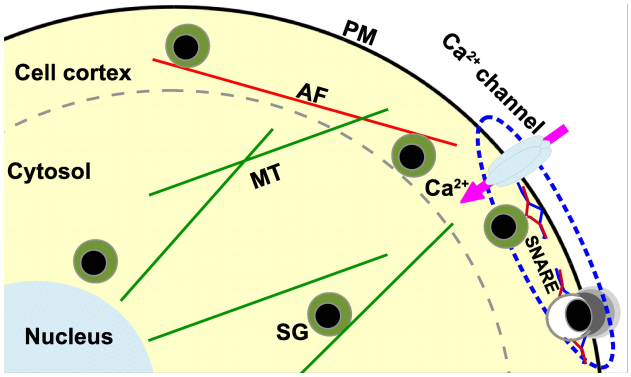

Figure 1: Diagram of the β-cell model. *Three compartments are distinguished in the cell: nucleus, cytosol and cell cortex. The cytosol and cortex are separated by the grey dashed line. Microtubules (MTs) are concentrated in the cytosol but can extend into the cortex, where actin filaments (AFs) are the guiding structures for the secretory granules (SGs). The arrow represents Ca^{2+} influx through an open Ca^{2+}-channel. The blue dashed line wraps around a series of the events at a docking site on the plasma membrane (PM) (see text).*

shell 0.6 µm thick beneath the PM. At this distance from the PM, the density of SGs was increased substantially- (Figure 5d in Fava *et al.* (37)). Below the cell cortex, the cytoskeleton is made of microtubules (MTs) only. The model β-cell contains S_0 = 6000 SGs in the resting state. The total SG number is not constant in the model but reflects homeostasis in a flow equilibrium of SG generation and loss. SG biosynthesis, degradation and exocytosis are mechanisms influencing the homeostasis and dynamics of SG numbers.

B. Size distribution of granules

SGs are spheres with different diameters. The SG size (diameter) distribution was sampled from the measured size distribution (Figure 3 in Fava *et al.* (37)), leading to an average SG size of d_{gr} = 243 nm.

C. SG biosynthesis and degradation

SGs are synthesized on demand to keep the total number of SGs in homeostatic level. In the

model, biosynthesis is incorporated as the rate at which new SGs carrying mature insulin are introduced to the cytoplasm; processes preceding synthesis are ignored. The rate *r(t)* at time *t* depends on deviations from the homeostatic SG number:

$$r(t)=r_0+(r_{max}-r_0)\times\frac{S_0^2-S^2(t-\tau_b)}{S_0^2}$$, where

$r_0 \approx 4$ SG/min and $r_{max} = 15$ SG/min are, respectively, the background (at basal glucose) and maximum synthesis rates, *S(t)* is total the SG number at time *t* and S_0 is the homeostatic number of SGs. The SG biosynthesis rate is assumed to be independent of the K^+ level. In the Golgi apparatus, preproinsulin is loaded to newly synthesized SGs in around 30 min. Accordingly, SG synthesis takes $\tau_b = 30$ min in the model, thus, introducing an adaptation delay to deviations from homeostasis (42).

In live cells, SGs have finite a life-time before degradation by autophagy or crinophagy through the lysosomal machinery. To find the SGs' half-life T_h we consider a Hill-function for the probability $p_d=\frac{a^2}{a^2+T_h^2}$ of a SG to have died at age *a*. According to this function, we assign a lifetime for each SG upon biosynthesis, which determines how long that specific SG will live in the model cell. In isolated rat islets at a fasting glucose level, $p_d = 30–40\%$ of the insulin is degraded in $a_0 = 24$ h (43, 44). Therefore, $T_h=a_0\sqrt{(1-p_d)/p_d}$ is 29.4–36.7 h according to the range of p_d given above. $T_h = 33$ h is used in the model and the lifetime of SGs is truncated at $4T_h$. This is close to the SG half-life of ≈30 h assumed in earlier studies (45). This SG degradation mechanism leads to an exponential decay in SG numbers in the reference system, when the biosynthesis of new SGs is blocked.

D. SG trafficking

To mimic the impact of the cytoskeleton network on SG motility, MTs and AFs are implicitly included in the model and determine the direction of SG motion. *In vivo*, MTs and AFs are oriented mainly (not perfectly) normal and tangential to the PM, respectively. The direction of the MTs in the model can deviate randomly from the radial direction to a maximum of 30°. The tangential movement of SGs on the AF is represented in spherical coordinates as changed polar and azimuthal angles while keeping the radial distance to the cell centre fixed. As AFs are not perfectly tangential *in vivo*, random movements in the radial direction are assumed, representing the deviation of AFs from the tangential orientation (±30°).

SGs exhibit two types of movements (46, 47): small random movements and longer excursions. In the model, each SG undergoes random movements for ≤3 min (46), which leads to <1 μm net displacement from its initial position, in agreement with experimental findings (47). The length of the subsequent excursion on MTs is a random value (≤2 μm) and occurs with equal probability towards or away from the PM (46). The excursion length is shorter for SGs moving on AFs, as the TIRFM data show that most of SGs can move for only ≤0.5 μm, on average, in a given direction in the cortical region (45). The SG alternatively switches between random and directed (excursion) movements, but not at every time-step. Upon starting an excursion or a random movement, the length or duration of the motion, respectively, are sampled from a uniform distribution. The SG switches to the next motion type only after completing the preceding one.

Although MTs are mainly present in the non-cortical region, they can also be found in the cortex. Therefore, in the model, a SG moving on a MT can enter the cell cortex at the end of its excursion and start a random motion there. Similarly, a SG which starts random movements outside the cortex can enter the cell cortex after 2 min of random motions. At the end of their random motions, these SGs which

were on a MT beforehand will switch to an AF, with a probability (p_{MA}) that increases from 0.1 at the edge of the cortex to 0.5 at the PM. This is assumed to mimic the increasing abundance of AFs compared to MTs in the cortex. Randomly moving SGs which were on AFs beforehand will switch to MTs at the end of their random motion, with a probability q_{MA}, which varies from 0.1 close to the PM to 0.5 at the edge of the cortex.

The overall picture of SG dynamics is as follows: A SG undergoes excursion on a MT. It then performs a random motion. After this random motion, if the SG is still in the non-cortical region, it restarts this process by switching to excursion on a new MT. If the SG is in the cortical region, it can switch to an AF, with a probability that depends on its distance from the PM. After excursion on an AF, the SG starts a random motion again. Depending on its position, the SG starts an excursion on a new AF or MT at the end of the random motion.

E. Granule speed as a function of glucose level

The speed of SGs depends on the intracellular glucose level (38, 47–49). This is because the ATP level increases in response to glucose stimulation, and this facilitates the motion of the motor proteins displacing intracellular vesicles, particularly SGs (48). In the unstimulated state, no saltatory SG movements are observed *in vivo* (46). However, at high glucose levels, SG trafficking is saturated, which is implemented as a Hill-function for the glucose dependency of SG speed during directed movements:

$$v_{av}(g) = v_{max} \times \frac{g}{g + g_{half}} \qquad (1)$$

where v_{max} = 0.5 µm/s is the maximum SG speed observed in TIRFM experiments (45), g is the glucose level and g_{half} is the glucose level at which the SG speed becomes half-maximum. g_{half} is determined from the measured SG mean speed (v_0 = 0.2 µm/s) in the presence of basal glucose (g_0 = 3 mM), corresponding to an unstimulated state (38, 49), where $g_{half} = g_0 \times v_{max}/v_0 - g_0$. During random movements, SGs are slower (46) (with a speed of v_{rnd}). In the model, v_{rnd} = 0.04 µm/s is assumed, which can increase up to 15% in the stimulated state, because *in vivo* random SG movement is only marginally affected by glucose (47).

The time-step of the agent-based model is δt = 1 s in the unstimulated state and shorter in the stimulated state when SGs are moving faster. The time-step is adapted so that no SG moves more than its average SG size (d_{gr} = 243 nm) per time-step. δt = 1 s is finer than the typical time-steps (5–10 s) used in experiments to capture images for analysis of SG dynamics (46, 47). In the unstimulated state (δt = 1 s and v_{rnd} = 0.04 µm/s), the root mean square of SG displacement, D_{rms}, over 1 min under mere random movements accounts to ≈0.31 µm (1.3 times the SG size). Considering the space occupied by SGs, this leads to a functional cage 0.86 µm in diameter ($2 \times D_{rms} + d_{gr}$), in agreement with experimentally reported values of 0.8–0.9 µm (46, 47, 50). This distance is calculated assuming that diffusion is without constraints: $D_{rms} = l\sqrt{N_s}$, where N_s = 60 is the number of SG steps of length l = 0.04 µm over 1 min. In the stimulated state, where shorter time-steps are adapted because of higher SG speeds, l remains constant and the number of steps per minute (N_s) increases, which leads to a net increase in D_{rms} and hence larger SG random movements (46).

F. Docking sites

In live cells, SGs dock to specific places on the PM, which are limited in number (51) and are in close contact with Ca^{2+}-channels (50, 52). This ensures that SGs are exposed to high levels of Ca^{2+} in the vicinity of channels (1). Measurements show 450 channels per cell, with several Ca^{2+}-channels associated with a single SG, forming a functional unit (53), called a docking site (DS) here. Analyses propose that most of DSs consist of Ca^{2+}-channel triplets,

and each DS is associated with a single SG (53). Therefore, in the model, we assume $\overline{N}_{bg}=150$ DSs (Ca^{2+}-channel triplets) on the PM at a basal glucose level. Each DS is a complex of m = 3 channels. The DSs are randomly distributed on the PM, and they do not overlap. Each DS occupies a circular area of one SG in diameter (d_{gr}) on the PM. Every SG can dock to an unoccupied DS if its surface is nearer than 10 nm to the DS (1, 17, 52). The docked SGs then either undergo exocytosis or detach from the DS on the PM. The half-time after which a SG will detach from a DS is assumed to be 10 min, based on the observation that some previously docked SGs undergo exocytosis 15 min after stimulation (17). There is no pre-defined SG pool in the model. Nevertheless, the docked and primed SGs (II.H) are interpreted as the RRP in the model, following the established definition in the literature (52, 53) (IV.C).

In vivo, glucose causes a rapid increase in the rate of protein synthesis in pancreatic β-cells (42, 54, 55), in addition to insulin release. These glucose-induced physiological changes can lead to changes in the exocytotic capacity of the cell. The number of DSs can increase via over-expression or via segregation of the channels or SNARE proteins which were clustered prior to glucose stimulation (56). In the model, the number of DSs is updated at every time-step i by taking the integer part of N_i:

$$N_i = N_{i-1} + r_{ch} \times \frac{\overline{N}_{g,i} - N_{i-j}}{\overline{N}_{g,i}} \times \delta t \qquad (2)$$

with

$$\overline{N}_{g,i} = A_1 + A_2 \frac{1}{1+\left(g_h/g_i\right)^n} \qquad (3)$$

being the asymptotic number of DSs at glucose g_i at time-step i. The integer part of $N_{i\text{-}j}$ (j = 240) is the existing number of DSs on the PM j seconds before the i^{th} step. g_h = 11 mM is the glucose half-maximum concentration (39), and n = 4 is the Hill-coefficient. n is chosen such that at very low (g < 3 mM) and very high (g > 20 mM) glucose levels, $\overline{N}_g$ reaches its asymptotic regime. The parameters A_1 = 148 and A_2 = 404 are fitted to maintain $\overline{N}_{bg}=150$ (see above) and $\overline{N}_{sg}=550$ (see III.C.1) at basal and saturating (30 mM) glucose levels, respectively. $r_{ch}=\frac{\overline{N}_{sg}-\overline{N}_{bg}}{30\,min}$ is the maximum rate of DS number adaptations (see III.C.1). When a new DS is introduced to the PM (see below), it is randomly positioned on the PM. Conversely, only unoccupied DSs are removed from the PM (in response to reduced glucose, in Eq. (2). If all the DSs are occupied at time-step i, N_i is not updated.

G. Calcium channels dynamics at the docking sites

In vivo, glucose stimulation results in PM depolarization, the opening of voltage-gated Ca^{2+}-channels and calcium influx. The present model does not consider ion currents explicitly but uses a phenomenological Hill-function to determine the opening probability of a Ca^{2+}-channel (p_1) at a given glucose (g): $p_1=\frac{g}{g+g_h}$. When all m Ca^{2+}-channels are closed, the DS will not conduct Ca^{2+}, which prohibits the fusion of primed SGs. The probability that Ca^{2+} is conducted by at least one channel of the DS is:

$$P = 1 - q_1^m \qquad (4)$$

where $q_1 = 1\text{-}p_1$ is the probability of a single channel closing. The time required for glucose metabolism is implemented with a 1-min delay of glucose sensing.

β-cells can also be stimulated by extracellular K^+. We consider stimulation with high K^+ concentrations, inducing PM depolarization and opening of voltage-gated Ca^{2+}-channels. Furthermore, we assume the application of diazoxide, which opens K_{ATP}-channels (57). The K^+ level determines the opening probability of

Ca^{2+}-channels similar to glucose level, with a half-maximum concentration of 16 mM. The time course of SG priming and exocytosis does not differ between K^+- and glucose-stimulations. Their differences are that K^+-stimulation is independent of glucose metabolism, thus stimulating without delay, and K^+ neither affects the speed of SGs (II.D), nor promotes DS (II.F) and SG biogenesis (II.C).

H. Priming

A docked SG has to get primed before exocytosis. Parts of the priming process, in reality, might happen before docking to the PM. However, due to a lack of knowledge on its exact molecular nature (1) and time-course, the complete SG priming is assumed to be a post-docking step in the model. For SGs in the model, the probability of priming (p) t seconds after docking follows a Hill-function $p=\frac{t}{t+\tau_p}$. τ_p is the priming half-time. For each docked SG, a random number $0<p<1$ is chosen to determine its priming time:

$$t_p=\tau_p\frac{p}{1-p} \qquad (5)$$

If not detached or degraded, the SG acquires a primed state after this time. The value of τ_p will be determined to match experimental secretion rates (see III.B.1). Docked and primed SGs may be unprimed. As no time scale for this process is known, we assumed that unpriming is associated with SG detachment.

I. Exocytosis

In our model, a primed SG fuses with the PM when at least one of the Ca^{2+}-channels of the hosting DS is open (II.G). When no Ca^{2+}-channel of the hosting DS is open, the SG remains docked until it is degraded (II.C) or detached from the PM (II.F), or undergoes exocytosis after a Ca^{2+}-channel opens. Measurements of secreted insulin (1, 40, 52) and visualisation of exocytosis events (16, 17) showed that stimulated secretion leads to a delayed secretion, not an immediate secretion, as induced by Ca^{2+} photorelease. Therefore, the SG exocytosis rate is phenomenologically modelled by fitting to the time-course of primed SGs' exocytosis at DSs of single β-cells (15, 17). A Hill-function with a Hill-coefficient of n = 3 and a half-maximum time of τ_{ex} (III.B.1) is assumed to describe the latency of DSs in conducting the exocytosis of primed SGs. This makes up a bell-shaped distribution, centred at $t = \tau_{ex}$, for latent exocytosis of primed SGs (see III.B.1 and Figure 4).

J. Number of β-cells per islet

The current model addresses insulin secretion from a single β-cell. In the experiments, secretion is measured in whole pancreas or islet instead of single cells. To compare our results with experimental data, we use the recent estimation of 3.5 fg of insulin ($\approx 3.5 \times 10^5$ insulin molecules) per SG (37). We also need to assume a number of cells per islet. This is done by comparing the first-phase peaks in simulations and experiments. However, the amplitude of the first-phase peak varies significantly among different experiments: 70 (19), 150 (39) and 200 (58) pg/min/islet (mouse islets, at 15 mM glucose). Most prominently, K^+-induced secretion from mouse islets in the absence of glucose peaks 30% higher than in the presence of 3 mM glucose (see Figures 4-B and 4-D in Henquin *et al.* (19)). Therefore, we have assumed different numbers of cells per islet: 1900 (Figures 4-A and 5-A), 1550 (Figures 4-B and 5-B) and 2100 (Figure 6). Table 1 summarises the parameters, constant values and sources used in the model.

III. Results

A. Steady state of the model β-cell

The model β-cell is evolved at a basal glucose level until homeostasis is reached. Starting from zero SGs, the β-cell reaches a steady state after 17 h. The steady state is a balance of insulin biosynthesis (with a rate of r_{max}), background insulin secretion and intracellular

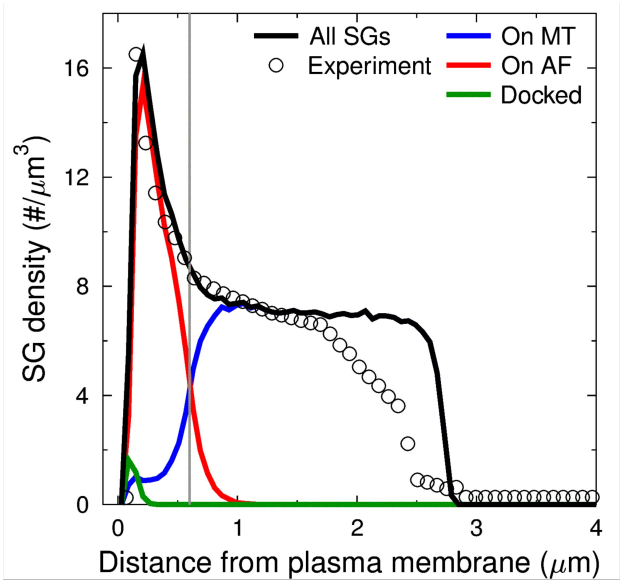

***Figure 2:* Secretory granule (*SG) density profile.** *The SG density is shown as a function of the distance from the plasma membrane (PM) in the equilibrated state of an unstimulated model β-cell. The black line shows the overall SG density, whereas the blue, red and green lines show the densities of SGs on* the microtubules *(MT),* on the actin filaments *(AFs) and docked to the PM, respectively. The simulation (black) is compared to experimental data (37) (circle). The grey line delineates the cortical region.*

SG degradation. The β-cell is evolved further for seven more days, which corresponds to five times the half-life of a SG, so that SGs of different ages are present. In the unstimulated state, it has ~135 docked SGs, ~120 of which are primed. This equilibrium state of the β-cell is used as the initial configuration for all simulations addressed in this study.

The emerging steady-state density profile of SGs as a function of the distance from the PM is shown in Figure 2. SGs are distributed uniformly in the cytosol and reach a maximum density of ≈17 μm^{-3} under the PM. In the model, SGs do not detect any physical barrier crossing from the non-cortical to the cortical region (grey line) but exhibit different motility on MTs and AFs, which dominate the non-cortical and the cortical region, respectively (see II.D). The tangential motion of SGs and their much smaller radial movement on AFs, which might guide SGs back to the non-cortical region, suggests that SGs spend more time in the cortex and accumulate under the PM. This leads to the density profile in Figure 2, which is in agreement with experimental results (37). The experimentally measured density profile decreases more smoothly in the vicinity of the nucleus. We attribute this deviation to organelles located in the vicinity of the nucleus, like the Golgi apparatus, which act as space restrictions and are neglected in the model β-cell. Since the innermost parts of the cytosol represent a tiny fraction of the total cell volume and we are mainly interested in the dynamics in the vicinity of the cortical region, this deviation (8% of the cytosol) is neglected. The model is considered to be suitable for an analysis of the dynamic intracellular spatial organization of SGs.

B. Model validation by β-cell stimulation

Starting from the resting model β-cell above, we now proceed to apply stimulation protocols in order to reproduce known biphasic insulin secretion patterns (1). The unknown parameters τ_{ex} and τ_p are determined by insulin secretion data from different experimental protocols of β-cell stimulation (19). The estimated τ_{ex} and τ_p values (below) will be used in all simulations, unless otherwise mentioned.

1. Continuous K^+-stimulation

The model β-cell was continuously stimulated with high K^+ (30 mM) for 60 min in the absence of glucose (Figure 3-A). A monophase (first phase-like) insulin secretion was induced, with a sharp initial peak followed by a decreasing tail. As secreted SGs are already primed, the first-phase peak position and width can be tuned by the secretion latency, τ_{ex}. With τ_{ex} = 3.5 min, the peak is in good agreement with experimental results (Figure 3-A). The

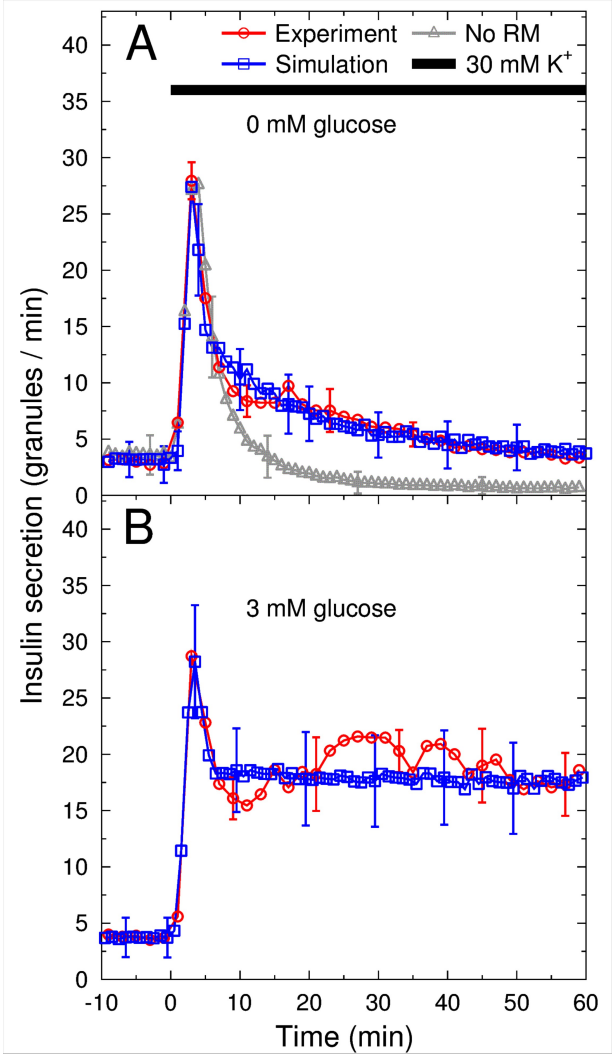

Figure 3: Continuous K^+-stimulation of a β-cell. A) *Insulin secretion from a β-cell in response to continuous stimulation with 30 mM K^+ in the absence of glucose. For comparison, the same simulation in the absence of random movements (RM) of secretory granules (SG) is shown (grey), (see IV.E).* ***B)*** *The same stimulation as in A, but in the presence of 3 mM glucose. The simulations (blue) are compared to experiment (red). Experimental data have been reproduced from Henquin et al. (19). In A and B, 1900 and 1550 β-cells per islet are assumed respectively. Error bars represent the standard deviations of 100 simulations.*

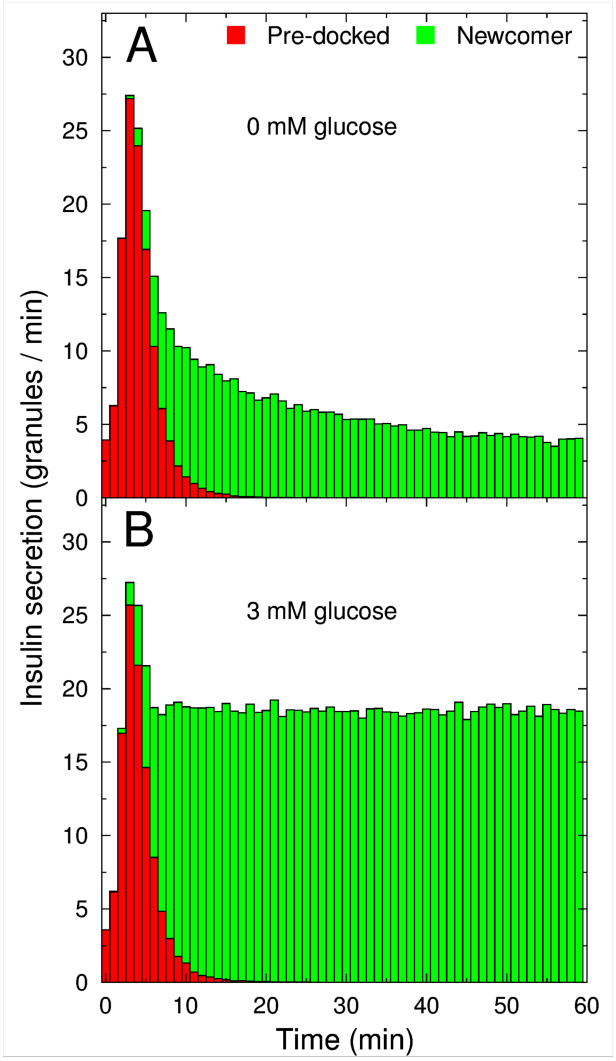

Figure 4: Contribution of pre-docked and newcomer secretory granules (SGs) to secretion phases. *Secretion profile of a β-cell stimulated by 30 mM K^+ in the (A) absence and (B) presence of basal glucose (as in Figure 3). The red and green bars show pre-docked and newcomer SGs, respectively.*

secretion rate peaks 3–4 min after stimulation, and then decreases quickly over a further 2 min before switching to a much slower reduction speed. After 60 min, the background secretion rate is reached again. The same experiment in the presence of 3 mM glucose, induces a peak of the same height (~28 SG/min) and at the same position (see II.J for a different number of cells used in 0 and 3 mM glucose scenarios). The secretion rate decreases for 2–3 min and then equilibrates above the background secretion rate. The secretion rate after

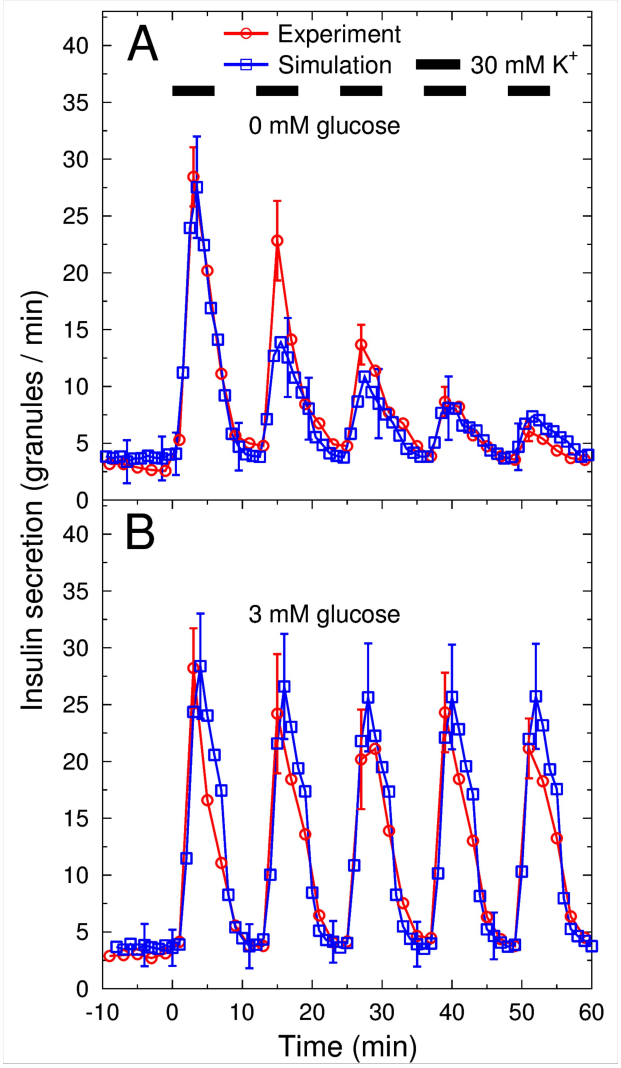

Figure 5: Intermittent K^+-stimulation of a β-cell. ***A)*** *Insulin secretion from a β-cell in response to an intermittent K^+ stimulation (periods of 6 min every 12 min) in the absence of glucose.* ***B)*** *The same stimulation with 3 mM glucose. The simulations (blue) are compared to experimental data (red). Experimental data have been reproduced from Henquin et al. (19). In A and B, 1900 and 1550 β-cells per islet are assumed, respectively. Error bars represent the standard deviations of 100 simulations.*

equilibration is controlled by the priming time and is in agreement with experimental results for $\tau_p = 30$ s (Figure 3-B).

Figure 4 shows the contribution of the pre-docked and newcomer SGs to insulin secretion from the model β-cell during continuous K^+ stimulation in the absence and presence of glucose (as in Figure 3). Until 7 min after the stimulation, pre-docked SGs provide most of the secreted insulin. During the second phase, when the pre-docked SGs are depleted, newcomers become the main secretory source. Their exocytosis rate decreases over time, in the absence of glucose, due to a decreased number of primed SGs (Figure 4-A). However, in the presence of glucose, the rate of recruiting newcomer SGs plateaus (Figure 4-B).

2. Intermittent K^+-stimulation

Following Henquin *et al.* (19), we next stimulate β-cells by intermittent bursts of increased K^+ (periods of 6 min every 12 min). The corresponding simulation is done without further parameter fitting. In the absence of glucose, a sequence of first phase-like peaks appears (Figure 5-A). At the end of each stimulation period, the secretion rate is reduced, which reflects the discharge of primed SGs. During the 6 min of resting (no stimulation), the secretion rate decreases to the unstimulated background level (2 SGs/min). Upon the next stimulation, another peak is induced, albeit with a smaller amplitude than the preceding peak. According to the simulation, the resting phase allowed new SGs to dock to the PM by slow random movements, such that the pool of docked SGs partially recovered. Indeed, by switching off random SG motion, subsequent peaks are suppressed due to a lack of SG replenishment in the DSs (data not shown). However, the amplitude of the peaks becomes successively smaller because SG replenishment is not complete.

When the same stimulation is done in the presence of 3 mM glucose (Figure 5-B), secretion peaks of comparable amplitude appear. After each stimulation, the secretion rate is reduced because pre-docked SGs have been secreted. During the 6 min of rest at 3 mM

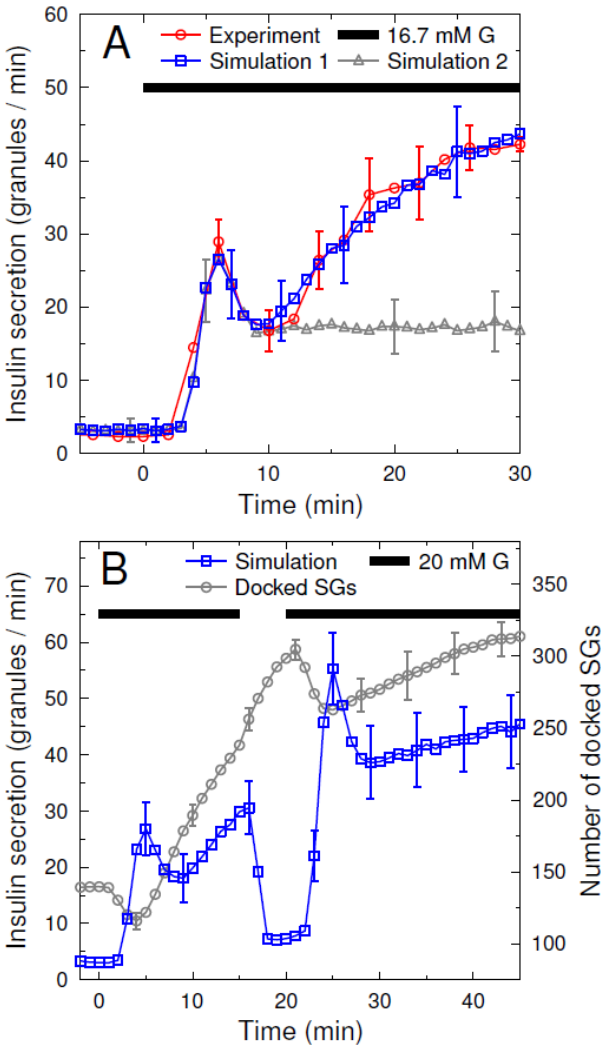

Figure 6: Secretion rate is controlled by the number of docking sites (DSs). A) *A delayed change in the DS number (from 150 at t = 0 to 445 at t = 30 min) upon stimulation with 16.7 mM glucose induces an increased exocytotic capacity and hence a rising second-phase insulin secretion rate. The simulation parameters (n and* $\overline{N}_{sg}$ *in Eqs. 2 and 3) were fitted to get the best agreement between the simulation (blue) and experimental data (red). The grey curve shows the same simulation for N = 150 DSs. The experimental data were reproduced from Straub et al. (59), assuming 2100 β-cells per islet.* ***B)*** *Insulin secretion in response to 20 mM glucose stimulations at time intervals of 0–15, and 20–45 min. The number of docked SGs during the same stimulation is also shown (right vertical axis). Error bars represent the standard deviations of 100 simulations.*

glucose, the pool of pre-docked SGs almost completely refills, leading to next peak being of comparable size. This shows that (>90%) refilling of docked SGs takes not more than 6 min at 3 mM glucose.

C. Modulation of the second-phase insulin secretion rate

In the previous section, the first phase of biphasic insulin secretion was discussed. In this section, the second phase is investigated and the influence of DS number and SG priming time are considered. For this purpose, the β-cell is stimulated by increased glucose. These two mechanisms are investigated separately to avoid intermixing their effects.

1. DS number

In this section, we ask how the number of DSs influences the insulin secretion rate *in silico*. The number of DSs in the model is updated according to Eqs. 2 and 3. The best agreement of simulation and experiment (Straub *et al.* (59)), as shown in Figure 6-A, was obtained by assuming $\overline{N}_{bg}=150$ (as in II.F) and $\overline{N}_{sg}=550$ (to have a consistent rise in the second-phase secretion rate). This corresponds to choosing A_1 = 148 and A_2 = 404. Upon stimulation with 16.7 mM glucose, the dynamic number of DSs turns an equilibrated (see below) second-phase secretion into a rising one (Figure 6-A). The second phase grows beyond the peak amplitude of the first phase. The number of docked SGs grows along with the number of DSs (from 150 at t = 0 to 445 at t = 30 min). This behaviour is also seen in experimental data (51), according to the same authors: an elevated glucose level leads to an increased number of docked SGs and an increasing second-phase secretion rate. These results suggest that the number of DSs may be a limiting factor of insulin secretion. When we turn off the glucose dependence of DS number in Eq. (3) and repeat the glucose stimulation, assuming 150 DSs on the PM, the second-phase secretion equilibrates at around ≈17.2 SG/min, (Figure 6-A, grey curve).

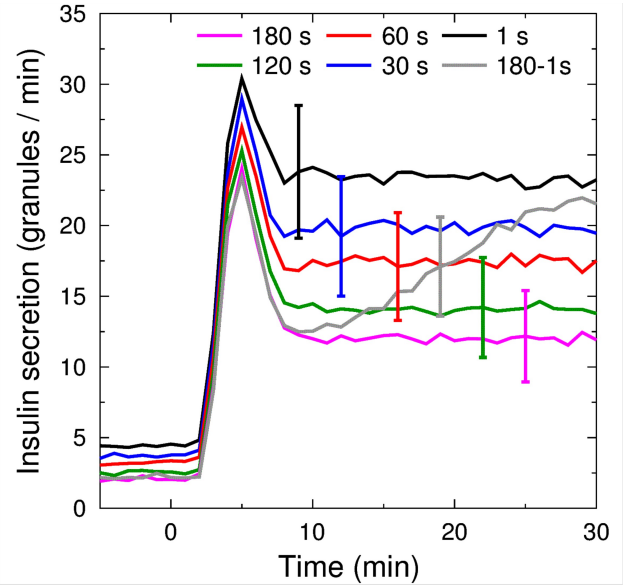

Figure 7: The second-phase secretion rate is controlled by the priming time. *The priming time, τ_p, is assumed constant with values ranging from 1 to 180 s. The model β-cell is stimulated with 20 mM glucose, while the number of docking sites (DSs) is kept constant at 150 and is the same in all simulations. All priming times induce a biphasic response with an equilibrated second phase. The priming time is assumed to change from 180 to 1 s between time 0 and 30 min, which induces a rising second phase (grey curve). Error bars represent the standard deviations of 100 simulations.*

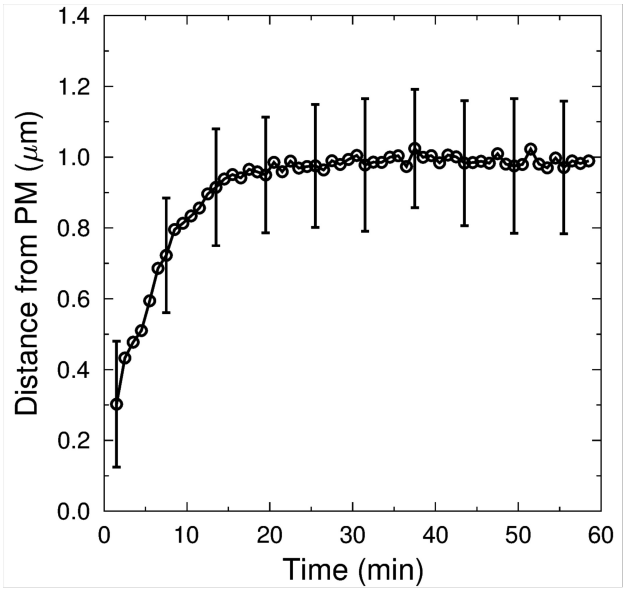

Figure 8: Pre-stimulation origin of newcomer* secretory granules (*SGs). *The model β-cell is stimulated with 20 mM glucose. At t = 0 the distance (d0) of SGs from the plasma membrane (PM) is saved. Every minute, d0 is averaged over SGs which completed the exocytosis process, resulting in a time course of the average distance from the PM of fused SGs at the time before stimulation. Error bars represent the standard deviations of 100 simulations.*

Glucose stimulation changes the number of DSs in a delayed manner. Therefore, if two similar stimulations are applied, with a short pause in between, they will induce different secretion profiles. We investigate this difference using the model. Upon the first glucose stimulation in silico, the second-phase secretion rate rises gradually (Figure 6-B). When the second stimulation begins after a short pause, the insulin response in both phases (starting at t = 20 min) becomes stronger than that of the first stimulation (starting at t = 0). This is due to the higher docking capacity. In the silent phase of the stimulation protocol (15–20 min), insulin secretion is still higher than background secretion (t<0), in agreement with the experimental data (23). This is because the number of DSs in the model β-cell adapts to the glucose level in a delayed manner.

2. Priming time

We investigate the influence of priming time, τ_p (Eq. (5)), on second-phase secretion by performing 20 mM glucose stimulations and assuming a constant number of 150 DSs. Different but constant priming times from 1 s to 3 min are assumed (Figure 7). Note that the background secretion level is slightly modified by this manipulation ($t \leq 0$). While the position and width of the first phase remain unchanged (no further tuning of τ_{ex} is required), its amplitude changes up to 25%. However, the second-phase insulin secretion rate clearly depends on τ_p: the shorter the priming time, the

greater the secretion. This shows that τ_p mostly controls the secretion rate during the second phase. For a constant priming time, however, the second-phase secretion rate never exceeds that of the first phase (Figure 7), even if the priming happens as quickly as 1 s. If τ_p is decreased from 180 s (at $t = 0$) to 1 s (at $t = 30$ min) following a modified Hill function with a Hill coefficient of 1 and a half maximum time of 10 min, the secretion rate grows during the second phase and becomes comparable to (but always less than) that of the first phase (Figure 7, grey curve). It should be noted that this is an *in silico* test and it is not clear whether or not the priming process can change that quickly *in vivo*. In short, unlike the number of DSs (III.C.1), modulation of the priming half-time cannot fully explain the rising second phase of insulin secretion, which grows beyond the first-phase peak (Figure 6-A). However, this does not exclude the possibility that both mechanisms are active.

D. Cytosolic origin of released SGs

In order to analyse the origin of newcomer SGs that are secreted upon glucose stimulation later on, the distance to the PM d_0 of each SG is saved at the time of stimulation ($t = 0$). The average value of d_0 for the SGs which have been fused in an interval of 1 min is monitored. Up to 6 min after stimulation, newcomers are mainly selected from SGs initially positioned in the cortical region (i.e. less than 0.6 µm from PM; Figure 8). The average origin distance of SGs increases with time and equilibrates at below 1 µm. This reflects the average distance of SGs from the PM in the homeostatic state (0.98 µm) weighted by the density profile in Figure 2. After 10 min, SGs are re-distributed within the β-cell and their chance to meet a free DS does not depend on their initial position any more. The origin of SG recruitment equilibrates at a distance outside of the cortex (0.6 µm). This proves that the SGs start from multiple locations and may point to a role of newcomers from not only the cortical region but also deep inside the cell.

IV. Discussion

A. SG dynamics control the SG density profile, priming and secretion

SG density in the cortical region is double that of the non-cortical region (37) in rat β-cells. In the model, the assumed granule dynamics control the cytosolic SG distribution. The cytoskeleton orientation and frequencies of directed and random movements differ between the cortical and non-cortical regions of the model β-cell. Therefore, SGs accumulate under the PM (see the density profile in Figure 2). When the model cytoskeleton is made up of only MTs, SGs uniformly occupy the cytosol (not shown here). Moreover, with the assumed granule dynamics, the SG speed controls the cortical SG density peak: Glucose induces faster SG dynamics, which enhances this peak.

K^+-stimulated secretion is suppressed in the absence of glucose (Figure 4-A, blue curve) due to the decreasing number of primed SGs. This shows that glucose (by employing SG dynamics) can affect the refilling rate of the primed SG pool. In reality, SG priming can be facilitated at the molecular level as well. Without excluding such a scenario, the post-docking priming of model SGs at the PM, modulated by SG dynamics, can reasonably explain the experimental data (Figure 4-A).

As the directed motion of SGs is lacking in the absence of glucose, only a limited number of newcomers are released upon stimulation (Figures 4-A and 5-A). According to the model, secretion declines further if SGs do not move randomly (Figure 3-A, grey curve). This shows that SGs that are close enough to free DSs to reach them by pure random movements make up the tail of the secretion profile (Figure 3-A, blue curve; $t \geq 6$ min), in the absence of glucose. At a basal glucose level, SGs acquire saltatory excursions and contribute more to

later secretion (Figures 4-B and 5-B). The recruitment rate of these newcomers remains unchanged over time at a basal glucose level (Figure 3-B, blue curve). This emphasises the relevance of a glucose-dependent SG dynamics model.

B. Stimulated secretion induces delayed exocytosis events

Capacitance measurements show that fusion pores open 20 ms after PM depolarization (53). However, insulin is released from primed SGs with a ≈1 min delay (time needed for glucose metabolism) and peaks 4–9 min later, as revealed by direct visualization of single SG exocytosis events using TIRFM (16, 17), as well as by traditional biochemical assays such as RIA, ELISA and carbon-fibre amperometry (1, 40, 52). This delayed (4–9 min) secretion compared to the early abundance of fusion events shows that stimulated secretions induce delayed exocytosis events. This latency (delay) is not a property of primed SGs, because it would contrast with their immediate release mentioned above. Such latency might be attributed to the exocytotic machinery or to the controversial role of remodelling of cortical F-actins (60). Although its molecular nature is still unknown, this latency turns out to be an important factor in the model. Therefore, the SG exocytosis rate is fitted in the model (II.I).

Exocytosis latency might also be attributed to delayed activation of the Ca^{2+}-channels or signalling pathways induced by different stimulation protocols. In the present model, we considered the possible role of delayed sensing of Ca^{2+} influx by primed SGs, due to their different distances from the Ca^{2+}-channels. This was tested by assuming 150 Ca^{2+}-channels (with the same conductance) on the PM and 600 docked SGs randomly distributed over the PM. Furthermore, we assumed a diffusion coefficient of $D=5\times10^{-6}\,cm^2/s$ for Ca^{2+} in the cytosol (61). We measured the time-lag between the opening of the Ca^{2+}-channels and the time-point when a SG experienced a threshold level of Ca^{2+}. This resulted in a distribution of time-lags (<0.4 s) that was much shorter than the completion of first-phase secretion (>4 min). Therefore, the Ca^{2+} dynamics were too fast to account for secretion latency, and we assumed that Ca^{2+} reached its quasi-steady state at each time-step of the simulation.

C. Functional subpopulations of SGs

Based on their fusion latency, different SG subsets are assumed in the literature. The RRP represents release-competent SGs which can undergo exocytosis without further modifications (1, 52, 62). In the model, we define RRP as pre-docked and primed SGs which undergo stimulated exocytosis. The size of RRP in the model depends on the number of DSs (N_{DS}), which is estimated from the measured number of Ca^{2+}-channel triplets (53). As shown in Figure 4-A (grey curve), 30 minutes of K^+-stimulation, with no glucose and no random motion of SGs, induces ≈190 exocytosis events. Under these conditions (no directed and random movement of SGs), in addition to the docked SGs, some undocked SGs are recruited if they are close enough (<10 nm) to the DSs that either have been free or became free during the stimulation. However, the unstimulated model β-cell has ~135 docked SGs, ~120 of which are primed and account for the RRP in the model. Depending on the experimental conditions, 50-200 SGs in RRP (14, 52, 53, 63) have been reported.

Morphologically docked SGs are traditionally defined as granules with a minimum distance of <10 nm from the PM, as seen in two-dimensional cell slices. Using this criterion, ~500–600 docked SGs per β-cell have been reported (1, 17). These estimations are based on ultrastructural analysis of proximity of SGs to the PM in a given static picture, which says nothing about their fate. Using proximity to the PM as a definition (SGs with shortest distance of <75 nm from the PM, as in TIRFM), our

model estimates >530 “morphologically docked” SGs in the unstimulated state, while only <150 of them are functionally docked to the PM and ~120 of them belong to the RRP. In other words,, in the model, morphologically docked SGs are >4 times more abundant than RRP SGs (1).

D. Biphasic secretion by the same exocytotic machinery

The temporal order in which the pre-docked and newcomer SGs appear in the secretion pattern, shown in Figure 4, has already been observed in experiments (16, 17, 64). Ohara *et al.* reported the involvement of two different classes of exocytotic proteins in the first and second phases of secretion (17). They showed that the docking and fusion of SGs are mainly Synt1A-dependent during the first phase but Synt1A-independent during the second phase. The model reproduces this temporal order by assuming the same exocytotic mechanism for both secretion phases (see Figure 4). Unlike previous models (26), no "highly calcium-sensitive pool of SGs" is assumed in the model to reproduce this temporal order. Instead, the dominance of pre-docked and newcomer SGs in the first and second phases, respectively, is a natural outcome of their availability to DSs. This is not in contrast to the experimental findings (17) mentioned above. It is likely that the different proteins involved in the exocytotic machinery play other roles than simply the regulation of secretion phases. In fact, experiments (16) have not shown different time-scales and kinetics for exocytosis events involving the two classes of proteins (17) mentioned above.

E. The pre-recruitment state of newcomer granules

The depth from which the newcomer SGs are recruited is unclear due to the limited view (in depth) of TIRFM. Due to their major contribution to the second phase of secretion, newcomers are generally believed to be stored intracellularly before translocation toward the PM and recruitment to the docked SG pool. Taking the intracellular SG dynamics into account , the current model sheds some light on the spatial origin of the newcomer SGs, which is not currently experimentally measurable.

The model predicts that the newcomers are mainly selected from areas beneath (<0.6 μm from) the PM until roughly 6 min after glucose stimulation. After 10 min, newcomers from whole cytosol (at $t = 0$) have an equal chance of secretion. New SGs are continuously biosynthesised in the model. Their travel from the vicinity of the nucleus to the PM can be as short as 15 s. Therefore, 10 min after the stimulation, the exocytosis of a newly synthesised SG is as likely as the exocytosis of a SG which was in the cytosol before the stimulation, according to the model.

Some experiments (17) show a greater (25%) contribution of the newcomers to the first phase (t < 7 min here) than what we found in the model (Figure 3). Other experiments (25) assign the majority of fusion events to newcomers that immediately undergo fusion, without being docked. In our model, newcomers with a very short (<2 s) docking state are responsible only for 5% of fusion events. Such differences are attributable to the limited view of TIRFM (<40 nm (25) or <100 nm (17)), which is too small to judge whether a SG (~240 nm) that suddenly appears in the visual field of the TIRFM was already close to PM but not docked or whether it was a considerable distance (e.g. one SG size) away from the PM.

F. Docking capacity causes insulin potentiation

Depending on the species and the experimental conditions, the secretion rate can rise during the second phase (19, 65, 66). The rising second-phase secretion rate is explained by increasing the number of DSs in the model (see III.C.1). This corresponds to increasing the docking capacity in real β-cells. It is likely that in

experiments where the second phase did not rise, docking capacity was not influenced by stimulation. This can be due to the experimental conditions or the physiology of the examined species.

When subsequent glucose stimulations are applied on real β-cells, the insulin response is amplified in both phases (3, 23, 24, 67). This effect, known as glucose potentiation of insulin secretion, declines if the silent interval between two stimuli is long enough: It has a half-life of 60–80 min in humans and ~20 min in rodents (24). The model reproduces the insulin potentiation effect by increasing the number of DSs under glucose stimulation (see Figure 6-B). If the silent phase between two stimuli is long enough, the number of DSs will equilibrate to a lower value at basal glucose levels and the potentiation effect will vanish (data not shown).

The rising second phase and potentiation of insulin secretion are explained by the same phenomenon: an increased number of DSs (in the model) or docking capacity (in real β-cells). The docking capacity *in vivo* can be increased by the turnover of different proteins involved in the exocytotic machinery. To further evaluate the role of the number of DSs in insulin potentiation, we propose an experiment in which the turnover of the exocytotic machinery is blocked. We expect that the potentiation effect will be suppressed, according to the model. Moreover, the model predicts that in experiments where the second-phase secretion rate does not rise, the subsequent stimulations will not be amplified.

As shown in III.C.2, for a given number of DSs, the secretion rate is further enhanced by lowering the priming half-time. This facilitated priming or "increased fusion rate of SGs at the PM" has been assumed to cause the potentiation effect in previous models (32). However, the facilitated priming fails to fully explain the glucose-induced insulin potentiation (see III.C.2), which can be as high as two- to four-fold greater than the first stimulation (24). With the existing experimental data, the docking and priming steps are not fully distinguishable. Therefore, from a mathematical point of view, we could unify them into a single state in the model, with a single delay time. Facilitated priming would then be translated to facilitated docking.

V. Summary and outlook

We present the first spatial model for SG dynamics in β-cells. SGs can move on the cytoskeletal components. There is only one SG pool in the model, unlike in previous models. However, SGs move differently in the cortical and non-cortical regions. Phenomenologically modelled SG dynamics leads to SG spatial organisation under the PM, similar to what has been seen in experiments (37) in the unstimulated state. Glucose stimulation leads first to exocytosis of docked SGs and then exocytosis of newcomers within ≤0.6 µm from the PM during the first 6 min. The model reproduces the biphasic stimulated insulin secretion with no need for having different exocytotic machinery for each phase and highly calcium-sensitive newcomers. The model provides the possibility to monitor the structural (SG-wise) changes of the β-cell caused by drugs which target the cytoskeleton network or exocytotic machinery. Moreover, SGs can be diverse in their mobility and docking competence, although we have considered one SG type in the model. Recent experiments have shown preferential exocytosis of newly synthesized insulin and age-dependent SG mobility (45), which might reflect the heterogeneity of SGs. The latter points will be addressed in future investigations.

Acknowledgements

This work was supported by the Helmholtz Association cross-program activity "Metabolic Dysfunction and Human Disease". No potential conflicts of interest relevant to this article were

reported. J.D. developed the model, designed the *in silico* experiments, analysed the data and wrote the manuscript. P.H., A.I., H.M. and A.M. contributed to discussions, and reviewed and edited the manuscript. Y.K. developed the Motion-Tracking software. M.S. contributed to discussions, and reviewed and edited the manuscript. M.M.H. contributed to discussions, designed the *in silico* experiments and wrote the manuscript. We thank the anonymous reviewers for their constructive criticisms that led to an improved final manuscript. J.D. thanks Gang Zhao, Klaus Knoch and Azadeh Ghanbari for many fruitful discussions.

References

1. Rorsman, P., and E. Renström. 2003. Insulin granule dynamics in pancreatic beta cells. Diabetologia. 46: 1029–45.

2. Rorsman, P., L. Eliasson, E. Renström, J. Gromada, S. Barg, and S. Göpel. 2000. The Cell Physiology of Biphasic Insulin Secretion. News Physiol Sci. 15: 72–77.

3. Caumo, A., and L. Luzi. 2004. First-phase insulin secretion: does it exist in real life? Considerations on shape and function. Am. J Physiol Endocrinol Metab. 287: E371–85.

4. Ohara-Imaizumi, M., and S. Nagamatsu. 2006. Insulin exocytotic mechanism by imaging technique. J. Biochem. 140: 1–5.

5. Wang, Z., and D.C. Thurmond. 2009. Mechanisms of biphasic insulin-granule exocytosis - roles of the cytoskeleton, small GTPases and SNARE proteins. J. Cell Sci. 122: 893–903.

6. Henquin, J.C. 2009. Regulation of insulin secretion: a matter of phase control and amplitude modulation. Diabetologia. 52: 739–51.

7. Pedersen, M.G., G. Cortese, and L. Eliasson. 2011. Mathematical modeling and statistical analysis of calcium-regulated insulin granule exocytosis in β-cells from mice and humans. Prog. Biophys. Mol. Biol. 107: 257–64.

8. Hosker, J., A. Rudenski, M. Burnett, D. Matthews, and R. Turner. 1989. Similar reduction of first- and second- phase B-cell responses at three different glucose levels in type II diabetes and the effect of gliclazide therapy. Metabolism. 38: 767–772.

9. Stefano Del Prato, A.T. 2001. The importance of first-phase insulin secretion: implications for the therapy of type 2 diabetes mellitus. Diabetes. Metab. Res. Rev. 17: 164–174.

10. Pratley, R.E., and C. Weyer. 2001. The role of impaired early insulin secretion in the pathogenesis of Type II diabetes mellitus. Diabetologia. 44: 929–45.

11. Guillausseau, P.-J., T. Meas, M. Virally, M. Laloi-Michelin, V. Médeau, and J.-P. Kevorkian. 2008. Abnormalities in insulin secretion in type 2 diabetes mellitus. Diabetes Metab. 34 Suppl 2: S43–8.

12. Eliasson, L., F. Abdulkader, M. Braun, J. Galvanovskis, M.B. Hoppa, and P. Rorsman. 2008. Novel aspects of the molecular mechanisms controlling insulin secretion. J. Physiol. 586: 3313–24.

13. Daniel, S., M. Noda, S. Straub, and G. Sharp. 1999. Identification of the docked granule pool responsible for the first phase of glucose-stimulated insulin secretion. Diabetes. 48: 1686–1690.

14. Olofsson, C.S., S.O. Göpel, S. Barg, J. Galvanovskis, X. Ma, A. Salehi, P. Rorsman, and L. Eliasson. 2002. Fast insulin secretion reflects exocytosis of docked granules in mouse pancreatic

B-cells. Pflugers Arch. 444: 43–51.

15. Ohara-Imaizumi, M., C. Nishiwaki, T. Kikuta, S. Nagai, Y. Nakamichi, and S. Nagamatsu. 2004. TIRF imaging of docking and fusion of single insulin granule motion in primary rat pancreatic beta-cells: different behaviour of granule motion between normal and Goto–Kakizaki diabetic rat beta-cells. Biochem. J. 381: 13–18.

16. Ohara-Imaizumi, M., Y. Nakamichi, T. Tanaka, H. Ishida, and S. Nagamatsu. 2002. Imaging exocytosis of single insulin secretory granules with evanescent wave microscopy: distinct behavior of granule motion in biphasic insulin release. J. Biol. Chem. 277: 3805–8.

17. Ohara-Imaizumi, M., T. Fujiwara, Y. Nakamichi, T. Okamura, Y. Akimoto, J. Kawai, S. Matsushima, H. Kawakami, T. Watanabe, K. Akagawa, and S. Nagamatsu. 2007. Imaging analysis reveals mechanistic differences between first- and second-phase insulin exocytosis. J. Cell Biol. 177: 695–705.

18. Zhu, D., Y. Zhang, P.P.L. Lam, S. Dolai, Y. Liu, E.P. Cai, D. Choi, S.A. Schroer, Y. Kang, E.M. Allister, T. Qin, M.B. Wheeler, C.-C. Wang, W.-J. Hong, M. Woo, and H.Y. Gaisano. 2012. Dual Role of VAMP8 in Regulating Insulin Exocytosis and Islet β Cell Growth. Cell Metab. 4: 238–249.

19. Henquin, J.-C., N. Ishiyama, M. Nenquin, M. a Ravier, and J.-C. Jonas. 2002. Signals and pools underlying biphasic insulin secretion. Diabetes. 51 Suppl 1: S60–7.

20. Curry, D.L., L.L. Bennett, and G.M. Grodsky. 1968. Dynamics of insulin secretion by the perfused rat pancreas. Endocrinology. 83: 572–84.

21. Grodsky, G.M. 1972. A threshold distribution hypothesis for packet storage of insulin and its mathematical modeling. J. Clin. Invest. 51: 2047.

22. E. Cerasi G. Fick, M.R. 1974. A mathematical model for the glucose induced insulin release in man. Eur. J. Clin. Invest. 4: 267–278.

23. O'Connor, M.D., H. Landahl, and G.M. Grodsky. 1980. Comparison of storage- and signal-limited models of pancreatic insulin secretion. Am. J. Physiol. 238: R378–89.

24. Nesher, R., and E. Cerasi. 2002. Modeling Phasic Insulin Release: Immediate and Time-Dependent Effects of Glucose. Diabetes. 51: 53–59.

25. Shibasaki, T., H. Takahashi, T. Miki, Y. Sunaga, K. Matsumura, M. Yamanaka, C. Zhang, A. Tamamoto, T. Satoh, J.-I. Miyazaki, and S. Seino. 2007. Essential role of Epac2/Rap1 signaling in regulation of insulin granule dynamics by cAMP. Proc. Natl. Acad. Sci. U. S. A. 104: 19333–8.

26. Pedersen, M.G., and A. Sherman. 2009. Newcomer insulin secretory granules as a highly calcium-sensitive pool. Proc. Natl. Acad. Sci. U. S. A. 106: 7432–6.

27. Bertuzzi, A., S. Salinari, and G. Mingrone. 2007. Insulin granule trafficking in β-cells: mathematical model of glucose-induced insulin secretion. Am. J. Physiol. Endocrinol. Metab. 293: 396–409.

28. Pedersen, M.G., A. Corradin, G.M. Toffolo, and C. Cobelli. 2008. A subcellular model of glucose-stimulated pancreatic insulin secretion. Philos. Trans. A. Math. Phys. Eng. Sci. 366: 3525–43.

29. Zhao, G., G. Dharmadhikari, K. Maedler, and M. Meyer-Hermann. 2014. Possible Role of

Interleukin-1β in Type 2 Diabetes Onset and Implications for Anti-inflammatory Therapy Strategies. PLoS Comput. Biol. 10: e1003798.

30. Fridlyand, L.E., and L.H. Philipson. 2011. Coupling of metabolic, second messenger pathways and insulin granule dynamics in pancreatic beta-cells: a computational analysis. Prog. Biophys. Mol. Biol. 107: 293–303.

31. Chen, Y., S. Wang, and A. Sherman. 2008. Identifying the targets of the amplifying pathway for insulin secretion in pancreatic beta-cells by kinetic modeling of granule exocytosis. Biophys. J. 95: 2226–2241.

32. Stamper, I.J., and X. Wang. 2013. Mathematical modeling of insulin secretion and the role of glucose-dependent mobilization, docking, priming and fusion of insulin granules. J. Theor. Biol. 318: 210–225.

33. Barg, S., M.K. Knowles, X. Chen, M. Midorikawa, and W. Almers. 2010. Syntaxin clusters assemble reversibly at sites of secretory granules in live cells. Proc Natl Acad Sci U S A. 107: 20804–20809.

34. Gandasi, N.R., and S. Barg. 2014. Contact-induced clustering of syntaxin and munc18 docks secretory granules at the exocytosis site. Nat. Commun. 5: 3914.

35. Zhu, D., E. Koo, E. Kwan, Y. Kang, S. Park, H. Xie, S. Sugita, and H.Y. Gaisano. 2013. Syntaxin-3 regulates newcomer insulin granule exocytosis and compound fusion in pancreatic beta cells. Diabetologia. 56: 359–69.

36. Axelrod, D. 2001. Total internal reflection fluorescence microscopy in cell biology. Traffic. 2: 764–74.

37. Fava, E., J. Dehghany, J. Ouwendijk, a Müller, a Niederlein, P. Verkade, M. Meyer-Hermann, and M. Solimena. 2012. Novel standards in the measurement of rat insulin granules combining electron microscopy, high-content image analysis and in silico modelling. Diabetologia. .

38. Baltrusch, S., and S. Lenzen. 2008. Monitoring of glucose-regulated single insulin secretory granule movement by selective photoactivation. Diabetologia. 51: 989–96.

39. Anello, M., P. Gilon, and J.C. Henquin. 1999. Alterations of insulin secretion from mouse islets treated with sulphonylureas: perturbations of Ca2+ regulation prevail over changes in insulin content. Br. J. Pharmacol. 127: 1883–91.

40. Bratanova-Tochkova, T.K., H. Cheng, S. Daniel, S. Gunawardana, Y.-J. Liu, J. Mulvaney-Musa, T. Schermerhorn, S.G. Straub, H. Yajima, and G.W.G. Sharp. 2002. Triggering and augmentation mechanisms, granule pools, and biphasic insulin secretion. Diabetes. 51 Suppl 1: S83–90.

41. Noske, A.B., A.J. Costin, G.P. Morgan, and B.J. Marsh. 2008. Expedited approaches to whole cell electron tomography and organelle mark-up in situ in high-pressure frozen pancreatic islets. J. Struct. Biol. 161: 298–313.

42. Knoch, K.-P., S. Nath-Sain, A. Petzold, H. Schneider, M. Beck, C. Wegbrod, A. Sönmez, C. Münster, A. Friedrich, M. Roivainen, and M. Solimena. 2014. PTBP1 is required for glucose-stimulated cap-independent translation of insulin granule proteins and Coxsackieviruses in beta cells. Mol. Metab. 3: 518–30.

43. Halban, P. a, and C.B. Wollheim. 1980. Intracellular degradation of insulin stores by rat pancreatic islets in vitro. An alternative pathway for homeostasis of pancreatic insulin content. J. Biol.

Chem. 255: 6003–6.

44. Sandberg, M., and L. a H. Borg. 2006. Intracellular degradation of insulin and crinophagy are maintained by nitric oxide and cyclo-oxygenase 2 activity in isolated pancreatic islets. Biol. cell. 98: 307–15.

45. Ivanova, A., Y. Kalaidzidis, R. Dirkx, M. Sarov, M. Gerlach, B. Schroth-Diez, A. Müller, Y. Liu, C. Andree, B. Mulligan, C. Münster, T. Kurth, M. Bickle, S. Speier, K. Anastassiadis, and M. Solimena. 2013. Age-dependent labeling and imaging of insulin secretory granules. Diabetes. 62: 3687–96.

46. Pouli, A.E., E. Emmanouilidou, C. Zhao, C. Wasmeier, J.C. Hutton, and G.A. Rutter. 1998. Secretory-granule dynamics visualized in vivo with a phogrin-green fluorescent protein chimaera. Biochem. J. 199: 193–199.

47. Ivarsson, R., S. Obermüller, G.A. Rutter, J. Galvanovskis, and E. Renström. 2004. Temperature-sensitive random insulin granule diffusion is a prerequisite for recruiting granules for release. Traffic. 5: 750–62.

48. Varadi, A., E. Ainscow, V. Allan, and G. Rutter. 2002. Involvement of conventional kinesin in glucose-stimulated secretory granule movements and exocytosis in clonal pancreatic β-cells. J. Cell Sci. 115: 4177–4189.

49. Hao, M., X. Li, M. a Rizzo, J. V Rocheleau, B.M. Dawant, and D.W. Piston. 2005. Regulation of two insulin granule populations within the reserve pool by distinct calcium sources. J. Cell Sci. 118: 5873–84.

50. Renström, E. 2011. Established Facts and Open Questions of Regulated Exocytosis in β-Cells – A Background for a Focused Systems Analysis Approach. In: Booß-Bavnbek B, B Klösgen, J Larsen, F Pociot, E Renström, editors. BetaSys: Systems Biology of Regulated Exocytosis in Pancreatic β-Cells. Springer New York. pp. 25–53.

51. Straub, S.G., G. Shanmugam, and G.W.G. Sharp. 2004. Stimulation of insulin release by glucose is associated with an increase in the number of docked granules in the beta-cells of rat pancreatic islets. Diabetes. 53: 3179–83.

52. Barg, S., L. Eliasson, E. Renström, and P. Rorsman. 2002. A subset of 50 secretory granules in close contact with l-type Ca2+ channels accounts for first-phase insulin secretion in mouse beta-cells. Diabetes. 51: S74–82.

53. Barg, S., X. Ma, L. Eliasson, J. Galvanovskis, S.O. Göpel, S. Obermüller, J. Platzer, E. Renström, M. Trus, D. Atlas, J. Striessnig, and P. Rorsman. 2001. Fast exocytosis with few Ca(2+) channels in insulin-secreting mouse pancreatic B cells. Biophys. J. 81: 3308–23.

54. Knoch, K.-P., H. Bergert, B. Borgonovo, H.-D. Saeger, A. Altkrüger, P. Verkade, and M. Solimena. 2004. Polypyrimidine tract-binding protein promotes insulin secretory granule biogenesis. Nat Cell Biol. 6: 207–214.

55. Gomez, E., M.L. Powell, I.C. Greenman, and T.P. Herbert. 2004. Glucose-stimulated protein synthesis in pancreatic beta-cells parallels an increase in the availability of the translational ternary complex (eIF2-GTP.Met-tRNAi) and the dephosphorylation of eIF2 alpha. J. Biol. Chem. 279: 53937–46.

56. Domanska, M.K., V. Kiessling, and L.K. Tamm. 2010. Docking and fast fusion of synaptobrevin

vesicles depends on the lipid compositions of the vesicle and the acceptor SNARE complex-containing target membrane. Biophys. J. 99: 2936–46.

57. Gembal, M., P. Detimary, P. Gilon, Z.Y. Gao, and J.C. Henquin. 1993. Mechanisms by which glucose can control insulin release independently from its action on adenosine triphosphate-sensitive K+ channels in mouse B cells. J. Clin. Invest. 91: 871–80.

58. Henquin, J.-C., M. Nenquin, A. Szollosi, A. Kubosaki, and A.L. Notkins. 2008. Insulin secretion in islets from mice with a double knockout for the dense core vesicle proteins islet antigen-2 (IA-2) and IA-2beta. J. Endocrinol. 196: 573–81.

59. Straub, S.G., and G.W.G. Sharp. 2004. The Two Phases of Glucose-Stimulated Insulin Secretion Mechanisms and Controls. In: LeRoith D, SI Taylor, JM Olefsky, editors. Diabetes Mellitus: A Fundamental and Clinical Text. Lippincott Williams & Wilkins. pp. 3–14.

60. Kalwat, M. a, and D.C. Thurmond. 2013. Signaling mechanisms of glucose-induced F-actin remodeling in pancreatic islet β cells. Exp. Mol. Med. 45: e37.

61. Donahue, B.S., and R.F. Abercrombie. 1987. Free diffusion coefficient of ionic calcium in cytoplasm. Cell Calcium. 8: 437–48.

62. Eliasson, L., E. Renström, W.-G. Ding, P. Proks, and P. Rorsman. 1997. Rapid ATP-dependent priming of secretory granules precedes Ca(2+)-induced exocytosis in mouse pancreatic B-cells. J. Physiol. 503: 399–412.

63. Smith, P. a, P. Proks, and F.M. Ashcroft. 1999. Quantal analysis of 5-hydroxytryptamine release from mouse pancreatic beta-cells. J. Physiol. 521 Pt 3: 651–64.

64. Nagamatsu, S., M. Ohara-Imaizumi, Y. Nakamichi, T. Kikuta, and C. Nishiwaki. 2006. Imaging docking and fusion of insulin granules induced by antidiabetes agents: sulfonylurea and glinide drugs preferentially mediate the fusion of newcomer, but not previously docked, insulin granules. Diabetes. 55: 2819–25.

65. Nunemaker, C.S., D.H. Wasserman, O.P. Mcguinness, I.R. Sweet, J.C. Teague, and L.S. Satin. 2006. Insulin secretion in the conscious mouse is biphasic and pulsatile. Am. J. Physiol. Endocrinol. Metab. 290: E523–29.

66. Henquin, J., M. Nenquin, P. Stiernet, and B. Ahren. 2006. In vivo and in vitro glucose-induced biphasic insulin secretion in the mouse: pattern and role of cytoplasmic Ca2+ and amplification signals in beta-cells. Diabetes. 55: 441–451.

67. Nesher, R., and E. Cerasi. 1987. Biphasic insulin release as the expression of combined inhibitory and potentiating effects of glucose. Endocrinology. 121: 1017–24.

VI. Tables

TABLE I: Parameter values used in simulations.

Symbol	Description	Value	Units	References
β-cell				
R	Cell radius	6	μm	Ref. (37)
R_n	Nucleus radius	3.1	μm	Ref. (37)
l_{ctx}	Thickness of cell cortex	0.6	μm	Ref. (37)
g_0	Basal glucose level	3	mM	Ref. (19)
g_h	Glucose half-maximum level	11	mM	*Ref (39)
τ_b	Time delay of insulin biosynthesis	30	min	Ref. (42)
A_1	Fitting parameter, Eq. (3)	148	-	Fitted
A_2	Fitting parameter, Eq. (3)	404	-	Fitted
SGs				
d_{gr}	Average SG diameter	243	nm	Ref. (37)
S_0	Homeostatic SG number	6000	-	Ref. (37)
r_{max}	Maximum SG production rate	15	/min	Assumed
T_h	SG half-life	33	h	*Refs. (43, 44)
τ_p	SG priming half-time	30	s	*Ref. (19)
τ_{ex}	SG exocytosis half-time	3.5	min	*Ref. (19)
v_{max}	Maximum SG speed	0.5	μm/s	Ref. (45)
v_0	SG speed at $g = g_0$	0.2	μm/s	Refs. (38, 49)
v_{rnd}	SG speed at random motion	0.04	μm/s	*Ref. (47)
t_{rnd}	Maximum duration of random motion	3	min	Ref. (46)
$l_{p,MT}$	Maximum length of excursion on MT	2	μm	Ref. (46)
$l_{p,AF}$	Maximum length of excursion on Af	0.5	μm	Ref. (45)
DSs				
$\overline{N}_{bg}$	Homeostatic number of DSs	150	-	*Ref. (53)
$\overline{N}_{sg}$	Maximum number of DSs	550	-	Fitted
r_{ch}	Maximum rate of DS number adaptation	13.3	/min	Assumed
d_{dock}	Minimum SG-DS distance for docking	10	nm	Ref. (1)
l_{ds}	Effective size of a DS	0.24	nm	Assumed
t_{dtch}	SG detachment half-time	10	min	*Ref. (17)
m	Ca^{2+}-channels per DS	3	-	Ref. (53)

*: Parameter value is estimated from the mentioned reference.